expression knockdown did not affect the antiviral activity of RO8191 or IFN-α, although IFN-γ activity was inhibited (Fig. 4c). These data suggest that, in addition to inducing similar gene expression, RO8191 and IFN-α exhibit similar STAT phosphorylation profiles. Although RO8191- and IFN-α-mediated antiviral activity remained constant when STAT1 expression was reduced, this could be because IFN-α signaling in HuH-7 cells requires minimal amounts of STAT1 protein and STAT1 expression was not reduced below such a critical threshold by siRNA in our system. In contrast, the inhibitory activity of RO8191 was attenuated to the same extent as that of IFN-α when the expression of other components of ISGF3 (STAT2 and IRF-9) were reduced by siRNA (Fig. 4d and e). Incidentally, STAT1 siRNA did not attenuate RO8191 or IFN activity in EMCV-infected A549 cells (supplementary Fig.14), which supports the notion that STAT2 is an essential component of type I IFN signaling[39]. Type I IFN stimulates the formation of other STAT-containing complexes, including STAT1:STAT1, STAT3:STAT3 and STAT5:STAT5 homodimers, as well as STAT1:STAT3 and STAT2:STAT6 heterodimers[40-42]. Like IFN, RO8191 induced the phosphorylation of STAT1 and STAT2, which function as a gateway to the type I IFN signal cascade, and stimulated the phosphorylation of STAT3, 5 and 6. Another possible cause for the fact that STAT1 knockdown did not show any effect on RO8191 inhibition could be compensation by these IFN signaling-stimulated STAT complexes. This finding matches the recent report by Perry *et al.* on the STAT dependency of IFN activity against Dengue virus, that belongs to flavivirus[43]. They showed that STAT2 mediates IFN antiviral signals even in STAT1 KO cells and they discussed the possibility that other STAT family proteins would compensate for STAT1 deficiency. In summary, with regards to the activation of transcription factors and ISG expression, RO8191 and IFN-α mediate the same pathway.

IFNs activate JAK kinases via IFN receptors to induce STAT phosphorylation. RO8191 robustly phosphorylated JAK1 (Fig. 2c) in comparison with IFN-α or -β and therefore we focused on IFNAR2 (a JAK1-binding subunit of the type I IFN receptor). As with IFN-α, the activity of RO8191 was inhibited by IFNAR2 knockdown (Fig. 3b). The suggestion that IFNAR2 is an essential molecule for RO8191-induced signal

transduction is supported by the fact that an IFNAR2-deficient cell line, U5A, did not respond to RO8191. Furthermore, after IFNAR2 expression had been complemented in the U5A cells, ISG induction by both RO8191 and IFN-α recovered (Fig. 3c and d). The mechanism was directly explained by SPR spectroscopy, which showed an interaction between RO8191 and the IFNAR2 ECD (Fig. 3e). RO8191 strikingly phosphorylates the IFNAR2-associated kinase JAK1, when compared to other IFN-treated cell lysates (Fig. 2c). JAK1 siRNA expression inhibited RO8191 activity (Fig. 4a), indicating that JAK1 is also an essential molecule for RO8191 activity. Interestingly, RO8191 activity remains static when IFNAR1 expression is knocked down, unlike IFN-α activity (Fig. 3b). The IFNAR1-binding-kinase Tyk2 is not required for RO8191 activity (Fig. 4b) and Tyk2 was not phosphorylated (Fig. 2c) by RO8191. Also, RO8191 induced its signal even in the Ifnar1 KO MEF and the Tyk2-deficient cell line (Supplementary Fig. 8 and 10). IFN-α induces a signal via IFNAR1/Tyk2 and IFNAR2/JAK1 but, although RO8191 and IFN-α induce common ISGs (Fig. 2b and Supplementary Fig. 2), RO8191 activity was dependent only on IFNAR2.

We therefore propose a novel model of the induction of IFN-like signal transduction by this small molecule (Fig. 4f). So far, the IFNAR2 homodimer has been suggested to play various roles in IFN signal transduction[34,44,45], and RO8191 would induce the ISG expression via such IFNAR2 homodimer. For type I IFN, both IFNAR1 and IFNAR2 cooperate and induce phosphorylation of STATs via JAK1 and Tyk2. Conversely, for RO8191, IFNAR2 alone, as a homodimer, activates JAK1 phosphorylation and subsequent STATs activation. Experiments using siRNA and deficient cells have also shown that IFNAR1 and Tyk2 were not required to induce antiviral activity in the RO8191 compound pathway. These findings suggest a novel aspect of the IFN signaling pathway that may contribute to the understanding of other molecular signaling in IFN pathways.

RO8191 is a small molecule whose oral administration is feasible and effective in a murine model (Table 1 and Supplementary Fig. 13). In the chimeric mice study, the anti-HCV effect of RO8191 and PEG-IFN was similar in that they both showed strong

activity at day 1 after treatment with subsequent weak suppression of HCV replication possibly due to the immunodeficiency of chimeric mice. Further development of RO8191 by using rational chemical modifications is therefore required to produce more potent molecules for testing as an antiviral molecule which will substitute current recombinant IFN. Although RO8191 has the potential to cause IFN-like adverse effects, further development of the small-molecule agonist offers the advantages of inexpensive production cost, convenient oral administration, dose-control to reduce some adverse effects, and potentially increased activity versus current recombinant IFNs.

Whereas oral NS3 protease inhibitors in monotherapy development yield resistant viruses[46,47], these protease inhibitors show a significantly high rate of SVR when combined with PEG-IFN[10,11] and a NS5B polymerase inhibitor also shows additive efficacy in combination with PEG-IFN[48]. In addition to the results of the *in vivo* study, we found that RO8191 induced ISGs at a level similar to IFN-α in human primary hepatocytes (Supplementary Fig. 4); we therefore expect that RO8191 will show IFN-like activity in clinical use. As an alternative strategy to protease/polymerase inhibitors with PEG-IFN, the combined use of these direct-acting antiviral agents with RO8191 in a new oral regimen may help overcome some of the delivery problems associated with current IFNs. SVR rates of individuals infected with HCV genotype 1 have increased from 5-20% with IFN monotherapy and up to 50% with a combination of IFN and ribavirin. However, the refractory patients in this therapy constitute an unmet medical need. Thus, the development of a novel IFN receptor agonist, used alone or in combination with direct-acting antiviral drugs, will add a new milestone to the treatment of chronic hepatitis C. In addition to HCV infection, type I IFNs have been approved for the treatment of multiple clinical conditions, including hairy cell leukemia, malignant melanoma, AIDS-related Kaposi's sarcoma, multiple sclerosis, and chronic hepatitis B[49]. Thus, R08191 shows strong potential as a lead compound for IFN substitutes.

Methods

Cell culture, mice, and reagents.

The #Huh7/3-1 cell line, which expresses HCV replicons, was a kind gift from F. Hoffmann-La Roche. The cells were cultured in 0.5 mg/mL G418-containing Dulbecco's modified Eagle's medium (DMEM, GIBCO) supplemented with 10% fetal bovine serum (FBS, HyClone). The replicon construct was derived from pFK-I377neo/NS3-3□/WT, as previously reported[19]. Hc cells (DS Pharma Biomedical) were cultured in CSC Complete Defined Serum-Free Medium (Cell Systems Corporation) supplemented with SF4ZR-500-D Rocket Fuel. Tlr KO MEFs were purchased from OrientalBioService, Inc. Ifnar1 KO MEF was kindly gifted by Prof. Takaoka. 2fTGH, and U1A and U5A cells were kindly gifted by Prof. Stark. Culture conditions for the other cell lines are shown in Supplementary Table 5. Six-week-old C57BL/6J mice were obtained from Charles River Laboratories. Chimeric mice harboring a functional human liver cell xenograft were purchased from PhoenixBio. The protocol was reviewed by the Institutional Animal Care and Use Committee of Chugai Pharmaceutical Co., Ltd. and all mouse experiments were performed in accordance with the Guidelines for the Accommodation and Care of Laboratory Animals promulgated in Chugai Pharmaceutical Co., Ltd. Recombinant human IFN-α2a was a kind gift from F. Hoffmann-La Roche. Recombinant murine IFN-αA and human IFN-β1a were purchased from PBL Interferon Source. Recombinant TNF-α and IFN-γ were purchased from R&D Systems. Imiquimod was purchased from LKT Laboratories. JAK inhibitor I was purchased from Merck.

Luciferase assay.

Luciferase activity was quantified using the Steady-Glo Luciferase assay system (Promega) and the EnVision 2013 Multilabel Reader (PerkinElmer).

WST-8 assay.

The viability of drug-treated Huh-7 cells was determined using a WST-8 cell counting kit (Dojin Laboratories).

Real-time RT-PCR.

Total RNA was extracted using Rneasy (Qiagen), and cDNA was synthesized using a Transcriptor First Strand cDNA Synthesis Kit (Roche Applied Science). Gene expression was measured using the LightCycler 480 System and LightCycler 480 Probes Master (Roche Applied Science). The amplification used 50 cycles of: 95 °C for 5 min, 95 °C for 10 s, and 60 °C for 30s. Human β-actin or rodent glyceraldehyde 3-phosphate dehydrogenase (GAPDH; Applied Biosystems) expression was used as the endogenous reference for each sample. Primers and TaqMan probes for genes were designed using the Universal Probe Library Assay Design Center (Roche Applied Science; Supplementary Table 6). The probes used were from the Roche Universal Probe Library (Roche Applied Science). The samples were run in triplicate for each target gene, and each reference gene was used as an internal control.

Western blotting and immunostaining.

Cells were lysed in CelLytic M Cell Lysis Reagent (Sigma-Aldrich) containing Protease Inhibitor Cocktail (Sigma-Aldrich) and PhosSTOP (Roche Applied Science). Rabbit polyclonal antibodies against STAT1, STAT3, STAT6, pY701-STAT1, pY690-STAT2, pY705-STAT3, pS727-STAT3, pY694-STAT5, pY641-STAT6, pY1022/1023-JAK1, and pY1054/1055-Tyk2 were purchased from Cell Signaling Technology. Rabbit polyclonal antibodies against actin, STAT2 and STAT5 were purchased from Santa Cruz Biotechnology. Anti-Tyk2 rabbit polyclonal antibody was purchased from Upstate.

Anti-IFNAR1 mouse monoclonal (MAB245) and anti-IFNAR2 sheep polyclonal antibodies were purchased from R&D Systems. Anti-NS3, anti-NS5A, and anti-NS5B rabbit polyclonal antibodies were a kind gift from F. Hoffmann-La Roche. Anti-NS4A and anti-NS4B mouse monoclonal antibodies were a kind gift from the Tokyo Metropolitan Institute of Medical Science. Proteins were detected using the Odyssey Infrared Imaging System (LI-COR). For immunostaining analysis, the cells were fixed on a 35-mm glass-based dish (Iwaki) with 4% paraformaldehyde, blocked using 5% fetal bovine serum in phosphate-buffered saline, and then incubated with anti-NS3 and anti-NS4A antibodies. The cells were then washed and incubated with Alexa488-labeled anti-rabbit IgG and Alexa568-labeled anti-mouse IgG (Molecular Probes) and analyzed using confocal laser microscopy.

JFH-1 antiviral assay.

A cured K4 cell line derived from HuH-7 HCV replicon cells was maintained in DMEM supplemented with 10% fetal calf serum (FCS), high-glucose nonessential amino acids, and HEPES (Invitrogen). The JFH-1/K4 cell line, which was persistently infected with the HCV JFH-1 strain, was maintained under the same conditions as the cured K4 cell line. For the anti-HCV assay of JFH-1/K4 cells persistently infected with the JFH-1 strain, JFH-1/K4 cells were seeded in a 24-well tissue culture plate containing DMEM supplemented with 10% FCS, high-glucose nonessential amino acids, and HEPES (Invitrogen). After overnight incubation, serial dilutions of reagent in growth medium were added. After 72 h, total RNA was purified from the JFH-1/K4 cells using Isogene (Nippon Gene). HCV-RNA was quantified by real-time PCR as previously reported[50].

EMCV cytopathic effect assay.

This assay was performed on A549 cells seeded in a 96-well tissue culture plate containing DMEM supplemented with 10% FBS. After overnight incubation, the indicated concentrations of each reagent were added to the growth medium. After 12 h, 100 $TCID_{50}$/mL EMCV was added, and after another 48 h, viable cells were stained with 0.5% crystal violet. RNAi experiment using EMCV was also performed on A549 cells seeded in a 96-well tissue culture plate containing DMEM supplemented with 10% FBS. We transfected STAT1- or STAT2-siRNA to A549 cells, and after 72 h we infected EMCV to the cells and treated them with 1 μM RO8191 or 2 IU/mL IFN. After additional 48 h incubation, we evaluated the cell viability by staining with crystal violet.

GeneChip and data analysis.

Total RNA was extracted from 10^7 HCV replicon cells cultured for 8 h in the presence of 2 μM RO8191 or 4 IU/mL IFN-α with TRIzol Reagent (Invitrogen). Reverse transcription, RNA labeling (5 μg of total RNA), hybridization to Human Genome U133 Plus 2.0 Arrays (Affymetrix), and scanning were performed according to the manufacturer's instructions (Affymetrix, http://www.affymetrix.com). GC-RMA (GeneChip Robust Microarray Analysis) algorithms were used to generate scaled gene expression values. The fold change compared to untreated cells was calculated, and probe sets were selected for genes that were at least 2.0-fold upregulated in RO8191- and IFN-α-treated cells relative to the control cells.

RNA interference.

For all double-stranded RNAs, ON-TARGET Plus siRNA reagents (Dharmacon) were used (Supplementary Table 7). The siRNAs were transiently transfected using Lipofectamine RNAiMAX Transfection reagent (Invitrogen) according to the manufacturer's protocols for reverse transfection.

Plasmids and transfection.

ISRE and NF-κB reporter gene were purchased from Clontech. *IFNAR2* was cloned into a pCOS2 vector[51] harboring the EF1α promoter. Plasmids were transfected using FuGENE HD (Roche Applied Science) according to the manufacturer's instructions.

SPR measurements.

SPR binding studies were performed using a Biacore T100. Recombinant IFNAR2 ECD protein was purchased from R&D Systems. The protein (1 mg/mL) was diluted 1:20 with 10 mM sodium acetate buffer (pH 5.0) and mixed with 2 μM RO8191 for stabilization of the binding site. The mixture was immobilized on a Series S sensor chip CM7 using amine coupling. RO8191 and PEG-IFN-α2a (Chugai Pharmaceutical) were injected onto the sensor chip at a flow rate of 0.03 mL/min. Response curves were generated by subtraction of the background signal generated simultaneously on a control flow cell. Kinetic parameters were obtained by global fitting of the sensorgrams to a 1:1 model using Biacore T100 Evaluation Software, version 2.0.1.

Humanized liver mice study.

The chimeric mice were generated by transplanting human primary hepatocytes into severe combined immunodeficient (SCID) mice carrying the urokinase plasminogen activator transgene controlled by an albumin promoter[38]. The chimeric mice used in this study were applied from Inoue *et al.*[52], and had a high substitution rate of human hepatocytes. Six weeks after hepatocyte transplantation, patient serum containing 10^6 copies of HCV genotype 1b was intravenously injected into each mouse. HCV titer reached approximately 10^8 copies/mL and was stable after 4 weeks of HCV injection and persistently infected for 12 weeks. Here, we used mice after 5 weeks post infection and tested for 2 weeks. The mice were treated for 14 days with RO8191 30 mg/kg/day orally or PEG-IFN-α2a 30 μg/kg subcutaneously twice weekly. HCV RNA in serum was extracted using the acid guanidinium-phenol-chloroform method. Quantification of HCV RNA was performed using real-time RT-PCR based on TaqMan chemistry, as described[50]. HCV inoculations, drug administration, blood collection, and killing were performed under ether anesthesia. Blood samples were taken from the orbital vein and sera were immediately isolated. The protocols for animal experiments were approved by the local ethics committee. The animals received humane care according to NIH guidelines. Patients gave written informed consent before sampling.

1. Lavanchy, D. The global burden of hepatitis. *Liver Int.* **29**, 74–81 (2009).

2. Ghany, M. G., Strader, D. B., Thomas, D. L. & Seeff, L. B. Diagnosis, management, and treatment of hepatitis C: an update. *Hepatology*. **49,** 1335-74 (2009).

3. Zeuzem, S. Interferon-based therapy for chronic hepatitis C: current and future perspectives. *Nat Clin Pract Gastroenterol Hepatol.* **5,** 610–622 (2008).

4. Ge, D. *et al*. Genetic variation in IL28B predicts hepatitis C treatment-induced viral clearance. *Nature*. **461,** 399-401 (2009).

5. Suppiah, V. *et al*. IL28B is associated with response to chronic hepatitis C interferon-alpha and ribavirin therapy. *Nat Genet*. **41,** 1100-4 (2009).

6. Tanaka, Y. *et al*. Genome-wide association of IL28B with response to pegylated interferon-alpha and ribavirin therapy for chronic hepatitis C. *Nat Genet*. **41,** 1105-9 (2009).

7. Thomas, D. L. *et al.* Genetic variation in IL28B and spontaneous clearance of hepatitis C virus. *Nature.* **461,** 798-801 (2009).

8. Czepiel, J., Biesiada. G. & Mach, T. Viral hepatitis C. *Pol Arch Med Wewn.* **118,** 734–740 (2008).

9. Webster, D. P., Klenerman, P., Collier, J. & Jeffery, K. J. Development of novel treatments for hepatitis C. *Lancet Infect Dis.* **9,** 108–117 (2009).

10. Jacobson, I. M. *et al.* Telaprevir for previously untreated chronic hepatitis C virus infection. *N Engl J Med.* **364**, 2405-16 (2011).

11. Poordad, F. *et al.* Boceprevir for untreated chronic HCV genotype 1 infection. *N Engl J Med.* **364**, 1195-206 (2011).

12..Kwong, A. D., McNair, L., Jacobson, I. & George, S. Recent progress in the development of selected hepatitis C virus NS3.4A protease and NS5B polymerase inhibitors. *Curr Opin Pharmacol.* **8,** 522–531 (2008).

13. Stark, G. R. *et al.* How cells respond to interferons. *Annu Rev Biochem.* **67,** 227–264 (1998).

14. de Veer, M. J. *et al.* Functional classification of interferon-stimulated genes identified using microarrays. *J Leukoc Biol.* **69,** 912-20 (2001).

15. Pestka, S., Langer, J. A., Zoon, K. C. & Samuel, C. E. Interferons and their actions. *Annu Rev Biochem.* **56,** 727–777 (1987).

16. Uze, G., Lutfalla, G. & Gresser, I. Genetic transfer of a functional human interferon alpha receptor into mouse cells: cloning and expression of its cDNA. *Cell.* **60,** 225–234 (1990).

17. Novick, D., Cohen, B. & Rubinstein, M. The human interferon alpha/beta receptor: characterization and molecular cloning. *Cell.* **77,** 391–400 (1994).

18. Lohmann, V. *et al.* Replication of subgenomic hepatitis C virus RNAs in a hepatoma cell line. *Science.* **285,** 110–113 (1999).

19. Sakamoto, H. *et al.* Host sphingolipid biosynthesis as a target for hepatitis C virus therapy. *Nat Chem Biol.* **1,** 333–337 (2005).

20. Wakita, T. *et al.* Production of infectious hepatitis C virus in tissue culture from a cloned viral genome. *Nat Med.* **11,** 791–796 (2005).

21. Kneteman, N. M. *et al.* Anti-HCV therapies in chimeric scid-Alb/uPA mice parallel outcomes in human clinical application. *Hepatology.* **43,** 1346–1353 (2006).

22. Dash, S. *et al.* Interferons alpha, beta, gamma each inhibit hepatitis C virus replication at the level of internal ribosome entry site-mediated translation. *Liver Int.* **25,** 580–594 (2005).

23. Der, S. D., Zhou, A., Williams, B. R. & Silverman, R. H. Identification of genes differentially regulated by interferon alpha, beta, or gamma using oligonucleotide arrays. *Proc Natl Acad Sci U S A.* **95,** 15623–15628 (1998).

24. Hemmi, H. *et al.* Small anti-viral compounds activate immune cells via the TLR7 MyD88-dependent signaling pathway. *Nat Immunol.* **3,** 196–200 (2002).

25. Kawai, T. & Akira, S. Toll-like receptor and RIG-I-like receptor signaling. *Ann N Y Acad Sci.* **1143**, 1-20 (2008).

26. Yamamoto, M. *et al.* Role of adaptor TRIF in the MyD88-independent toll-like receptor signaling pathway. *Science.* **301**, 640-3 (2003).

27. Hoshino, K. *et al.* Cutting edge: Toll-like receptor 4 (TLR4)-deficient mice are hyporesponsive to lipopolysaccharide: evidence for TLR4 as the Lps gene product. *J Immunol.* **162**, 3749-52 (1999).

28. Hemmi, H. *et al.* A Toll-like receptor recognizes bacterial DNA. *Nature.* **408**, 740-5 (2000).

29. Mosca, J. D. & Pitha, P. M. Transcriptional and posttranscriptional regulation of exogenous human beta interferon gene in simian cells defective in interferon synthesis. *Mol Cell Biol.* **6**, 2279-83 (1986).

30. Diaz, M. O. *et al.* Homozygous deletion of the alpha- and beta 1-interferon genes in human leukemia and derived cell lines. *Proc Natl Acad Sci U S A.* **85**, 5259-63 (1988).

31. Chen, H. M. *et al.* Critical role for constitutive type I interferon signaling in the prevention of cellular transformation. *Cancer Sci.* **100**, 449-56 (2009).

32. Lutfalla, G. *et al.* Mutant U5A cells are complemented by an interferon-alpha beta receptor subunit generated by alternative processing of a new member of a cytokine receptor gene cluster. *EMBO J.* **14,** 5100–5108 (1995).

33. Velazquez, L. Fellous, M. Stark, G. R. & Pellegrini, S. A protein tyrosine kinase in the interferon alpha/beta signaling pathway. *Cell.* **70**, 313-22 (1992).

34. Lewerenz, M. Mogensen, K. E. & Uzé, G. Shared receptor components but distinct complexes for alpha and beta interferons. *J Mol Biol.* **282**, 585-99 (1998).

35. Shuai, K. *et al.* Interferon activation of the transcription factor Stat91 involves dimerization through SH2-phosphotyrosyl peptide interactions. *Cell.* **76,** 821–828 (1994).

36. Sarasin-Filipowicz, M. *et al.* Interferon signaling and treatment outcome in chronic hepatitis C. *Proc Natl Acad Sci U S A.* **105,** 7034–9 (2008).

37. Farnsworth, A. *et al.* Acetaminophen modulates the transcriptional response to recombinant interferon-beta. *PloS One.* **5,** e11031 (2010).

38. Mercer, D. F. *et al.* Hepatitis C virus replication in mice with chimeric human livers. *Nat Med.* **7**, 927-33 (2001).

39. Leung, S. *et al.* Role of STAT2 in the alpha interferon signaling pathway. *Mol Cell Biol.* **15,** 1312–1317 (1995).

40. Li, X. *et al.* Formation of STAT1-STAT2 heterodimers and their role in the activation of IRF-1 gene transcription by interferon-alpha. *J Biol Chem.* **271**, 5790–4 (1996).

41. Ghislain, J. J. & Fish, E. N. Application of genomic DNA affinity chromatography identifies multiple interferon-alpha-regulated Stat2 complexes. *J Biol Chem.* **271**, 12408–13 (1996).

42. Gupta, S. Jiang, M. & Pernis, A. B. IFN-alpha activates Stat6 and leads to the formation of Stat2:Stat6 complexes in B cells. *J Immunol.* **163**, 3834–41 (1999).

43. Perry, S. T., Buck, M. D., Lada, S. M., Schindler, C. & Shresta, S. STAT2 Mediates Innate Immunity to Dengue Virus in the Absence of STAT1 via the Type I Interferon Receptor. *PloS Pathogens*. **7**, e1001297 (2011).

44. Pattyn, E. *et al.* Dimerization of the interferon type I receptor IFNaR2-2 is sufficient for induction of interferon effector genes but not for full antiviral activity. *J Biol Chem.* **274**, 34838-45 (1999).

45. Platis, D. & Foster, G. R. Activity of hybrid type I interferons in cells lacking Tyk2: a common region of IFN-alpha 8 induces a response, but IFN-alpha2/8 hybrids can behave like IFN-beta. *J Interferon Cytokine Res.* **23**, 655-66 (2003).

46. McHutchison, J. G. *et al.* Telaprevir with peginterferon and ribavirin for chronic HCV genotype 1 infection. *N Engl J Med*. **360,** 1827-38 (2009).

47. Hézode, C. *et al.* Telaprevir and peginterferon with or without ribavirin for chronic HCV infection. *N Engl J Med*. **360,** 1839-50 (2009).

48. Kneteman, N. M. *et al.* HCV796: A selective nonstructural protein 5B polymerase inhibitor with potent anti-hepatitis C virus activity in vitro, in mice with chimeric human livers, and in humans infected with hepatitis C virus. *Hepatology*. **49,** 745-52 (2009).

49. Gutterman, J. U. Cytokine therapeutics: lessons from interferon alpha. *Proc Natl Acad Sci U S A.* **91,** 1198–1205 (1994).

50. Takeuchi, T. *et al.* Real-time detection system for quantification of hepatitis C virus genome. *Gastroenterology.* **116,** 636–642 (1999).

51. Yabuta, N. *et al.* Method for screening ligand having biological activity. PCT Int. Appl. WO0206838 (2002).

52. Inoue, K. *et al.* Evaluation of a cyclophilin inhibitor in hepatitis C virus-infected chimeric mice in vivo. *Hepatology*. **45**, 921-8 (2007).

Acknowledgments

This study was supported financially by Chugai Pharmaceutical Co., Ltd. H.K., K.O., Y.O., H.Y., H.O., M.A., A.O., H.S., N.H., A.K., K.M., T.T., N.S., Y.A., M.A. and M.S. are employees of Chugai Pharmaceutical Co., Ltd. We are grateful to George Stark for providing us the 2fTGH, U1A and U5A cell lines, and Akinori Takaoka for mouse Ifnar1-knockout MEFs. We also thank Isamu Kusanagi and Chiaki Tanaka for technical assistance, AVSS Co., Ltd. for technical assistance on EMCV, and Editing Services at Chugai Pharmaceutical Co., Ltd. for editorial assistance.

Author contribution statement

H.K., K.O., Y.O., H.Y., Y.H., A.O. and N.H. performed the experiments; H.K., K.O., H.O. and M.A. analyzed the data; G.F. and W.A. provided experimental materials and input into the data analysis; H.S., A.K., M.K., T.T., N.S., G.F., Y.A., M.A. and M.S. provided expert information; and H.K. and M.S. wrote the manuscript.

Additional information

Competing financial interests The author(s) declare no competing financial interests.

Figure Legends

Figure 1. Identification of a small molecule that inhibits HCV replication. (**a**) The chemical structure of RO8191. (**b**) After treatment with various concentrations of RO8191 or 100 IU/mL IFN-α for 72 h, HCV replication levels were examined using a luciferase assay (left graph), and cell viabilities were determined using a WST-8 assay (right graph). The mean values and their SDs were recorded for treated cells as a percentage of the values for untreated cells, and the values represent the means of 3 independent experiments. (**c**) Total RNA was extracted from HCV replicon cells cultured with the indicated concentration of RO8191 or 100 IU/mL IFN-α for 72 h; HCV RNA levels were analyzed using real-time RT-PCR. The mean values and their SDs were recorded for treated cells relative to the mRNA levels of β-actin, and are shown as a percentage of untreated cells. The values represent the means of 3 independent experiments. (**d**) HCV replicon cells were treated with control medium (left panels) or 10 μM RO8191 (right panels) for 24 h and immunostained with Hoechst 33452 (blue), anti-NS3 antibody (green), and anti-NS4A antibody (red). The results were then merged (yellow). (**e**) HCV replicon cells were treated with the indicated concentrations of RO8191 or 100 IU/mL IFN-α for 72 h. Whole cell lysates were immunoblotted with antibodies specific to the indicated HCV NS proteins. (**f**) After infection with the HCV JFH1 strain, Huh-7/K4 cells were treated with the indicated concentrations of RO8191 for 72 h. Total RNA was extracted, and the HCV RNA levels were analyzed using quantitative real-time RT-PCR.

Figure 2. RO8191 activates JAK/STAT and induces IFN-like signals. (**a**) The cytopathic effect of EMCV infection was inhibited by the indicated concentrations of RO8191 or IFN-α. Viable cells were stained with crystal violet. The data shown are the mean values and SDs based on experiments performed in quadruplicate. (**b**) ISG expression levels were measured using real-time RT-PCR. Total RNA was extracted from HCV replicon cells cultured in the presence of 50 μM RO8191 or 100 IU/mL IFN-α for 2 or 8 h and known ISGs were analyzed. Asterisk indicates 2-h treatment with agents. The values shown are the mean fold change induction compared to the mRNA level of human *β-actin* and the fold change induction compared to untreated cells. (**c**) HCV replicon cells were treated with various concentrations of the indicated agents for 15 min. Total lysates were immunoblotted with antibodies to STATs or JAK kinases. The HCV replicon IC_{50} of IFN-α was 0.4 IU/mL, that of IFN-β was 3 IU/mL, and that of IFN-γ was 0.3 ng/mL.

Figure 3. RO8191 requires and binds IFNAR2. (**a, b**) The anti-HCV replicon activity of RO8191 was attenuated by knockdown of IFNAR2 (**b**), but not IFNAR1 (**a**). Inhibition of HCV replicon replication by each agent is shown (the mean and SD from 3 experiments). The HCV replicon cells were transfected with 50 nM of the indicated siRNAs (blue, red, and yellow bars). Forty-eight hours after transfection, the HCV replicon cells were treated with 1.5 μM RO8191 or 3 IU/mL IFN-α for 24 h. Twenty-four hours after treatment with each agent, the replication levels of HCV RNA were analyzed using a luciferase assay. (**c, d**) U5A cells that lack IFNAR2 were transfected with either an empty vector or a vector expressing the *IFNAR2* gene. (**c**) Forty-eight

hours after transfection, the cells were treated with 50 μM RO8191 (red bars) or 100 IU/mL IFN-α (yellow bars). After an additional 8 h of incubation, total RNA was extracted from the U5A cells, and the *OAS1* mRNA level was measured using real-time RT-PCR. The values shown are relative to the mRNA level of human *β-actin*. (**d**) Forty-eight hours after transfection, the cells were lysed, and the whole cell lysates were immunoblotted with the indicated antibodies. (**e**) Real-time kinetic SPR analysis of the binding of RO8191 to the IFNAR2 ECD (red and blue lines). The results are consistent with 1:1 binding. PEG-IFN-α2a was also injected as a positive interacting control for IFNAR2 (black line, K_D: 30 nM). (**f**, **g**) The phosphorylation of STAT1 was attenuated by a knockdown of IFNAR2 (**g**) but not IFNAR1 (**f**). The HCV replicon cells were transfected with the indicated siRNAs (10 nM). Forty-eight hours after transfection, the cells were treated for 15 min with 10 μM RO8191 or 200 IU/mL IFN-α. The total lysates were subjected to western blot analysis to analyze the phosphorylated and total protein levels of STAT1. The data were statistically analyzed using Student's *t*-test.

Figure 4. RO8191 activates a novel IFN-like pathway. (**a–e**) The inhibition of HCV replicon replications by each agent is shown (mean and SD). The HCV replicon cells were transfected with 50 nM of the indicated siRNAs (blue, red, and yellow bars). (**a**, **b**) The anti-HCV replicon activity of RO8191 was reduced by knockdown of JAK1 (**a**) but not Tyk2 (**b**). Forty-eight hours after transfection, the HCV replicon cells were treated with 1.5 μM RO8191 or 3 IU/mL IFN-α. Twenty-four hours after treatment with each agent, the replication levels of HCV RNA were analyzed using a luciferase assay. (**c-e**) The anti-HCV replicon activity of RO8191 was reduced by knockdowns of STAT2 (**d**) and IRF9 (**e**), but not STAT1 (**c**). Forty-eight hours after transfection, the HCV replicon cells were treated with 1.5 μM RO8191, 3 IU/mL IFN-α, or 50 ng/mL IFN-γ. Twenty-four hours after treatment, the replication levels of HCV RNA were analyzed using a luciferase assay. (**f**) A schematic showing the pathways of RO8191 and IFN-α. The data were statistically analyzed using Student's *t*-test, and differences were considered significant at p values < 0.05.

Table 1. ISG expression in the livers of RO8191 treated mice. ISG expression levels were measured using real-time RT-PCR. Values are listed relative to the mRNA levels of rodent *Gapdh* and represent the mean fold change induction compared to vehicle-administered mice. Twenty-four hours after oral administration of 30 mg/kg RO8191 or vehicle (including 10% dimethyl sulfoxide and 10% Cremophor) to mice, total RNA was extracted from the mouse livers, and the mRNA levels of murine ISGs were measured using real-time RT-PCR. The data shown are the means and SDs of 4 mice per group. The data were statistically analyzed using Student's *t*-test, and differences were considered significant at p values < 0.05.

Table 1

Gene	Entrez ID	Fold change ± SD	p-value
murine Oas1	NM_001083925	3.0 ± 0.72	0.003
murine Mx1	NM_010846	2.1 ± 0.15	0.0003
murine Pkr	NM_011163	1.4 ± 0.21	0.009
murine Cxcl10	NM_021274	1.7 ± 0.63	0.097
murine Ifit3	NM_010501	2.5 ± 0.48	0.001

murine Isg15	NM_015783	2.3	±	0.41	0.002
murine Mda5	NM_027835	1.6	±	0.22	0.003
murine Rig-i	NM_172689	2.1	±	0.16	0.00003
murine Socs1	NM_009896	2.6	±	1.04	0.057
murine Stat1	NM_009283	1.8	±	0.21	0.001
murine Usp18	NM_011909	2.6	±	0.69	0.017

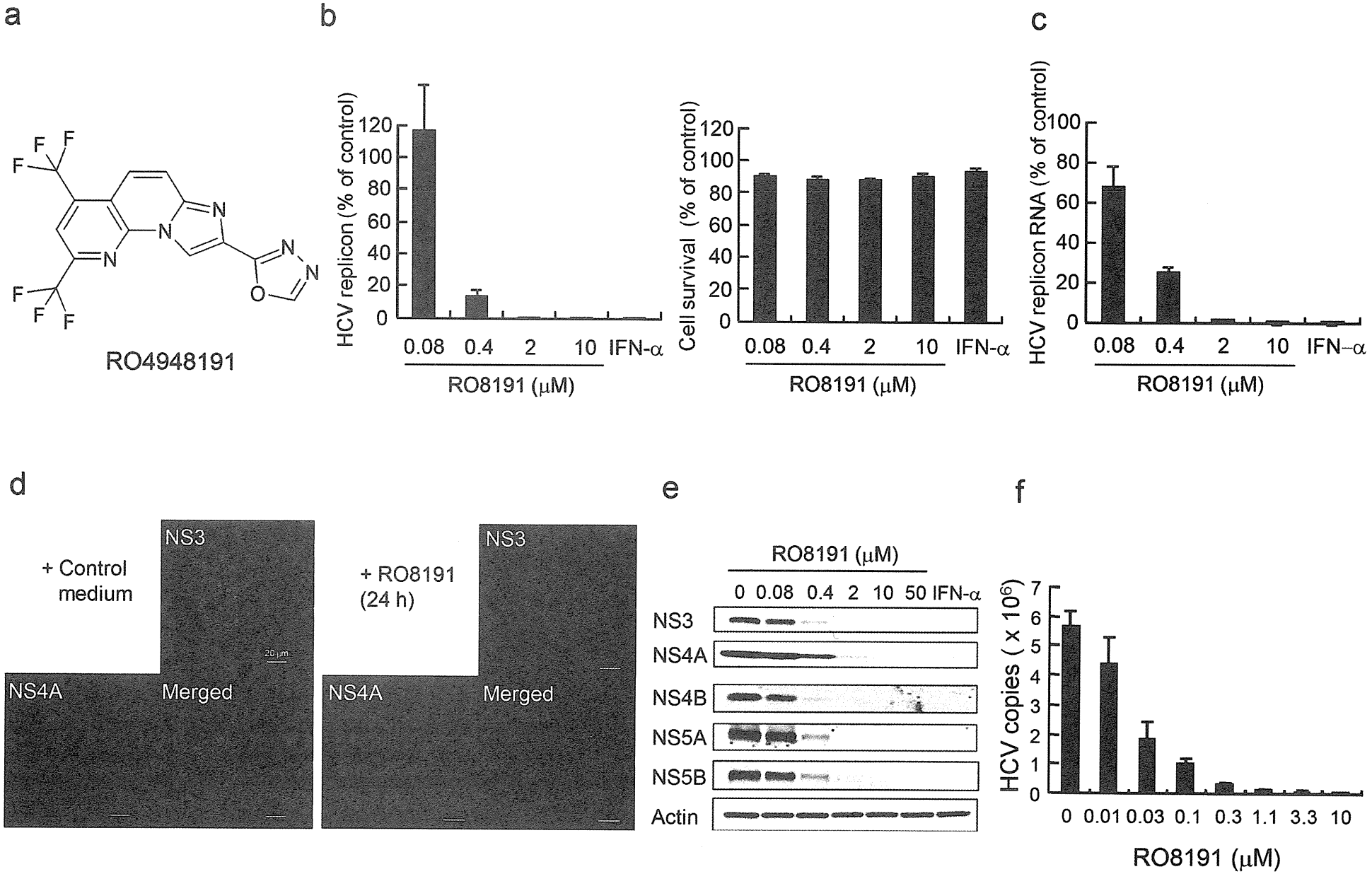
a
RO4948191
b
HCV replicon (% of control)
120
100
80
60
40
20
0
0.08 0.4 2 10 IFN-α
RO8191 (μM)
Cell survival (% of control)
120
100
80
60
40
20
0
0.08 0.4 2 10 IFN-α
RO8191 (μM)
c
HCV replicon RNA (% of control)
100
80
60
40
20
0
0.08 0.4 2 10 IFN-α
RO8191 (μM)
d
+ Control medium
NS3
NS4A
Merged
20 μm
+ RO8191 (24 h)
NS3
NS4A
Merged
e
RO8191 (μM)
0 0.08 0.4 2 10 50 IFN-α
NS3
NS4A
NS4B
NS5A
NS5B
Actin
f
HCV copies (x 10^6)
7
6
5
4
3
2
1
0
0 0.01 0.03 0.1 0.3 1.1 3.3 10
RO8191 (μM)

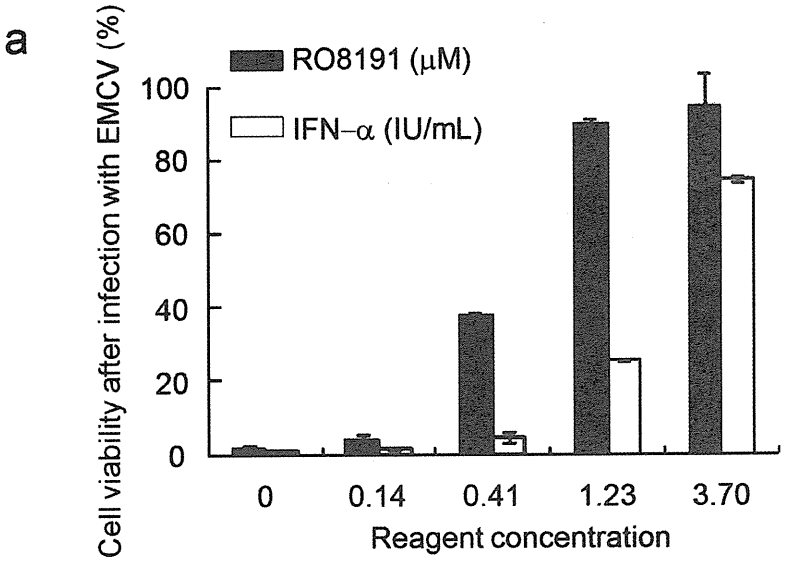
a
RO8191 (μM)
IFN–α (IU/mL)
Cell viability after infection with EMCV (%)
100
80
60
40
20
0
0
0.14
0.41
1.23
3.70
Reagent concentration

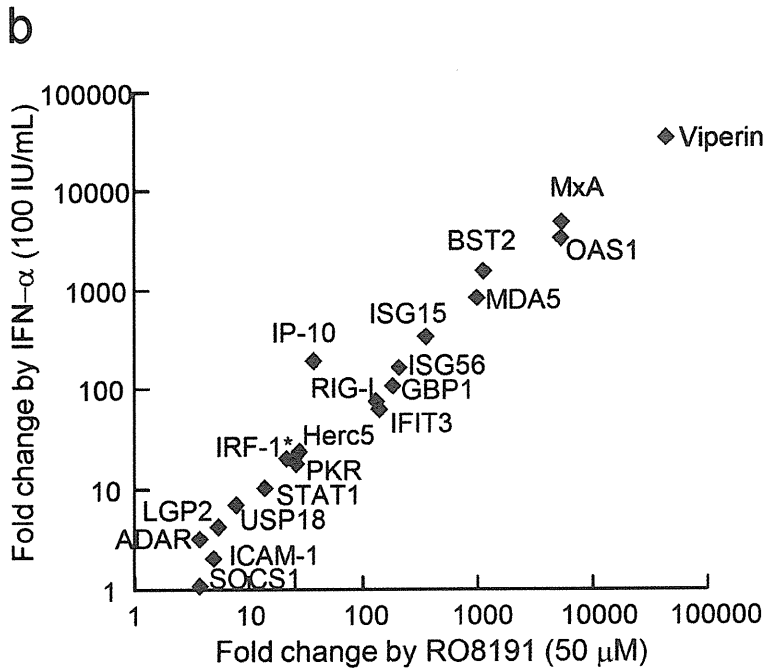
b
Fold change by IFN–α (100 IU/mL)
100000
10000
1000
100
10
1
Viperin
MxA
OAS1
BST2
MDA5
ISG15
IP-10
ISG56
RIG-I
GBP1
IFIT3
IRF-1*
Herc5
PKR
STAT1
LGP2
USP18
ADAR
ICAM-1
SOCS1
1
10
100
1000
10000
100000
Fold change by RO8191 (50 μM)

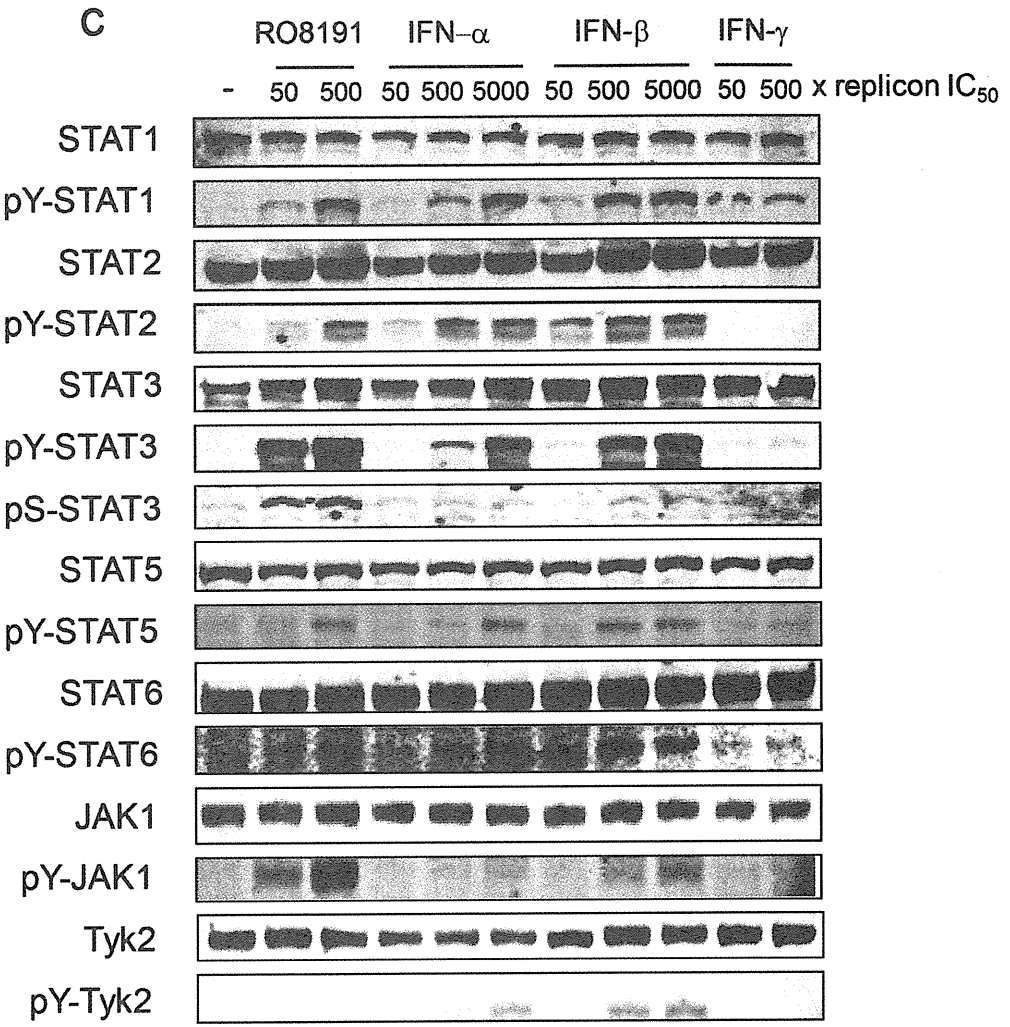
c
RO8191
IFN–α
IFN-β
IFN-γ
- 50 500 50 500 5000 50 500 5000 50 500 x replicon IC50
STAT1
pY-STAT1
STAT2
pY-STAT2
STAT3
pY-STAT3
pS-STAT3
STAT5
pY-STAT5
STAT6
pY-STAT6
JAK1
pY-JAK1
Tyk2
pY-Tyk2

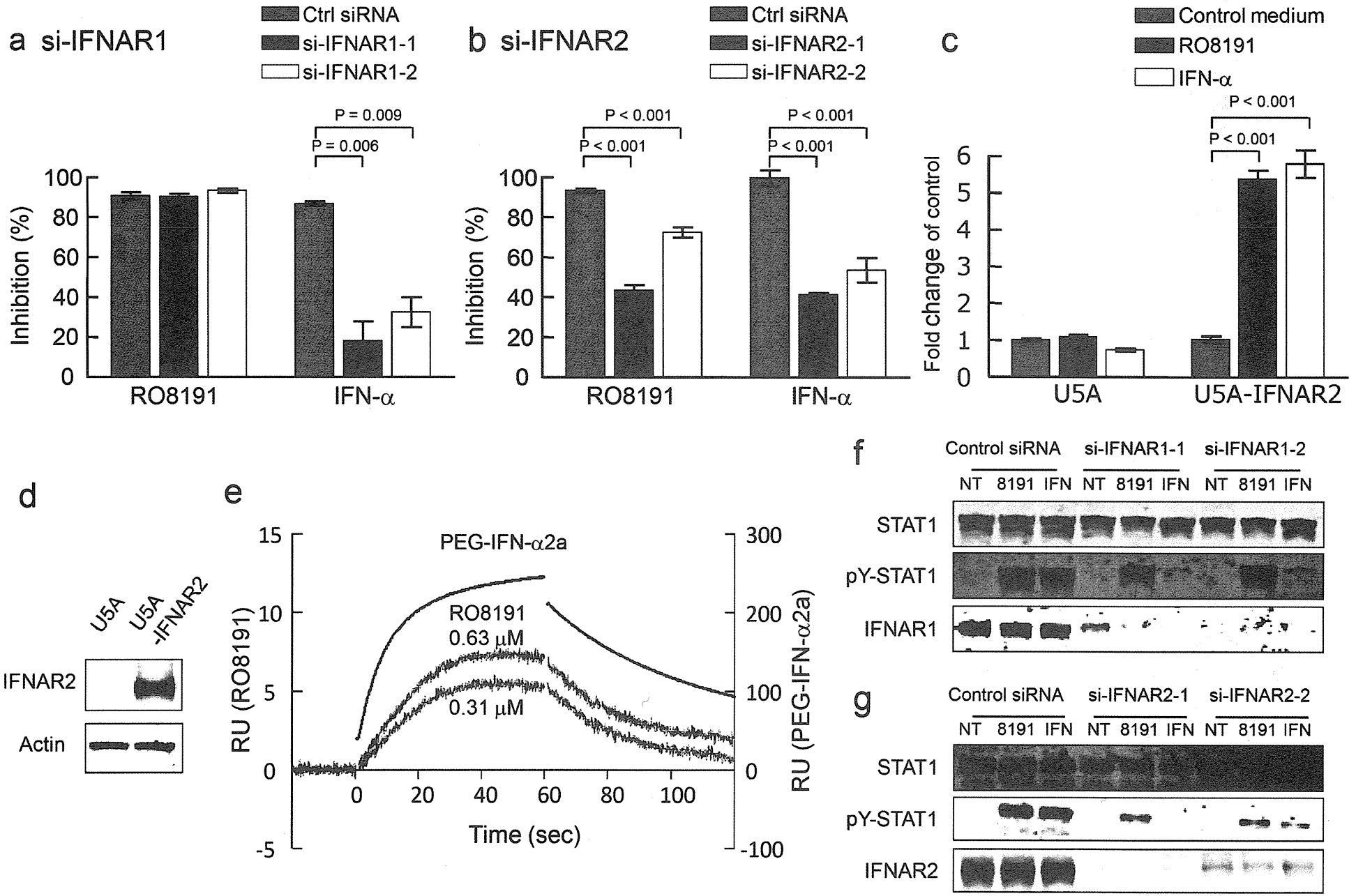
a si-IFNAR1
Ctrl siRNA
si-IFNAR1-1
si-IFNAR1-2
P = 0.009
P = 0.006
Inhibition (%)
RO8191
IFN-α
b si-IFNAR2
Ctrl siRNA
si-IFNAR2-1
si-IFNAR2-2
P < 0.001
P < 0.001
P < 0.001
P < 0.001
Inhibition (%)
RO8191
IFN-α
c
Control medium
RO8191
IFN-α
P < 0.001
P < 0.001
Fold change of control
U5A
U5A-IFNAR2
d
U5A
U5A -IFNAR2
IFNAR2
Actin
e
PEG-IFN-α2a
RO8191
0.63 μM
0.31 μM
RU (RO8191)
RU (PEG-IFN-α2a)
Time (sec)
f
Control siRNA
si-IFNAR1-1
si-IFNAR1-2
NT 8191 IFN NT 8191 IFN NT 8191 IFN
STAT1
pY-STAT1
IFNAR1
g
Control siRNA
si-IFNAR2-1
si-IFNAR2-2
NT 8191 IFN NT 8191 IFN NT 8191 IFN
STAT1
pY-STAT1
IFNAR2

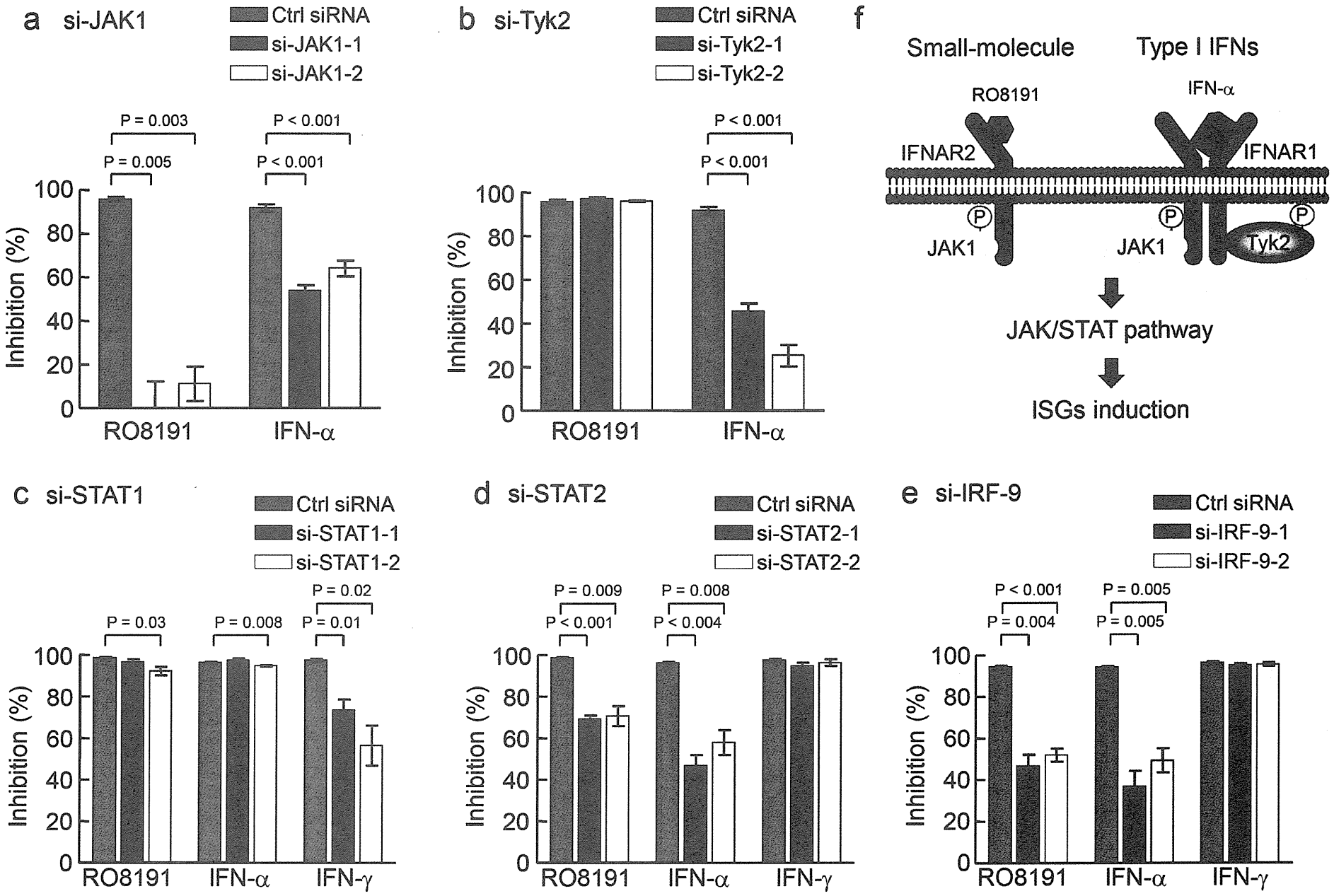
a si-JAK1
Ctrl siRNA
si-JAK1-1
si-JAK1-2
P = 0.003
P < 0.001
P = 0.005
P < 0.001
Inhibition (%)
100
80
60
40
20
0
RO8191
IFN-α
b si-Tyk2
Ctrl siRNA
si-Tyk2-1
si-Tyk2-2
P < 0.001
P < 0.001
Inhibition (%)
RO8191
IFN-α
f
Small-molecule
Type I IFNs
RO8191
IFN-α
IFNAR2
IFNAR1
JAK1
JAK1
Tyk2
JAK/STAT pathway
ISGs induction
c si-STAT1
Ctrl siRNA
si-STAT1-1
si-STAT1-2
P = 0.03
P = 0.008
P = 0.02
P = 0.01
Inhibition (%)
RO8191
IFN-α
IFN-γ
d si-STAT2
Ctrl siRNA
si-STAT2-1
si-STAT2-2
P = 0.009
P < 0.001
P = 0.008
P < 0.004
Inhibition (%)
RO8191
IFN-α
IFN-γ
e si-IRF-9
Ctrl siRNA
si-IRF-9-1
si-IRF-9-2
P < 0.001
P = 0.004
P = 0.005
P = 0.005
Inhibition (%)
RO8191
IFN-α
IFN-γ

JVI
Journals.ASM.org

The Toll-Like Receptor 3-Mediated Antiviral Response Is Important for Protection against Poliovirus Infection in Poliovirus Receptor Transgenic Mice

Yuko Abe,[a] Ken Fujii,[a] Noriyo Nagata,[b] Osamu Takeuchi,[c] Shizuo Akira,[c] Hiroyuki Oshiumi,[d] Misako Matsumoto,[d] Tsukasa Seya,[d] and Satoshi Koike[a]

Neurovirology Project, Tokyo Metropolitan Institute of Medical Science, 2-1-6 Kamikitazawa, Setagaya-ku, Tokyo 156-8506, Japan[a]; Department of Pathology, National Institute of Infectious Diseases, 4-7-1 Gakuen, Musashimurayama, Tokyo 208-0011, Japan[b]; Laboratory of Host Defense, WPI Immunology Frontier Research Center (IFReC), Osaka University, 3-1 Yamada-oka, Suita, Osaka 565-0871, Japan[c]; and Department of Microbiology and Immunology, Hokkaido University Graduate School of Medicine, Kita 15, Nishi 7, Kita-ku, Sapporo 060-8638, Japan[d]

RIG-I-like receptors and Toll-like receptors (TLRs) play important roles in the recognition of viral infections. However, how these molecules contribute to the defense against poliovirus (PV) infection remains unclear. We characterized the roles of these sensors in PV infection in transgenic mice expressing the PV receptor. We observed that alpha/beta interferon (IFN-α/β) production in response to PV infection occurred in an MDA5-dependent but RIG-I-independent manner in primary cultured kidney cells *in vitro*. These results suggest that, similar to the RNA of other picornaviruses, PV RNA is recognized by MDA5. However, serum IFN-α levels, the viral load in nonneural tissues, and mortality rates did not differ significantly between MDA5-deficient mice and wild-type mice. In contrast, we observed that serum IFN production was abrogated and that the viral load in nonneural tissues and mortality rates were both markedly higher in TIR domain-containing adaptor-inducing IFN-β (TRIF)-deficient and TLR3-deficient mice than in wild-type mice. The mortality rate of MyD88-deficient mice was slightly higher than that of wild-type mice. These results suggest that multiple pathways are involved in the antiviral response in mice and that the TLR3-TRIF-mediated signaling pathway plays an essential role in the antiviral response against PV infection.

Poliovirus (PV), which belongs to the genus *Enterovirus* in the family *Picornaviridae*, is the causative agent of poliomyelitis (38). The host range of PV is restricted to primates (18). This species' tropism is determined primarily by the cellular PV receptor (PVR; CD155), which gives the virus access to susceptible cells (14–16, 20). Mice are generally not susceptible to PV. However, transgenic mice expressing human PVR (PVR-tg mice) become susceptible to PV and develop a paralytic disease similar to human poliomyelitis after the administration of PV intravenously, intraperitoneally, intracerebrally, or intramuscularly but not orally (26, 40). PV shows a neurotropic phenotype in both humans and PVR-tg mice. PV preferentially replicates in neurons, especially in motor neurons in the anterior or ventral horn of the spinal cord and in the brainstem. However, the efficiency of PV replication is low in nonneural tissues (4, 25). We previously found that innate immune responses that are mediated by type I interferons (IFNs) play important roles in controlling viral replication in nonneural tissues and in the mortality rates of PVR-tg mice (19). In PVR-tg mice deficient in IFNAR1, PV efficiently replicates in nonneural tissues such as the liver, pancreas, and spleen, which are not normal targets of PV. IFNAR1-deficient mice die after the inoculation of a small amount of PV by peripheral routes. The results suggest that the type I IFN response forms an innate immune barrier that prevents PV replication in nonneural tissues and subsequent PV invasion of the central nervous system (CNS). This response therefore plays important roles in the tissue tropism and pathogenicity of PV (25).

The sensors that are involved in the production of type I IFNs in response to RNA viral infections have been recently identified and characterized (1, 46–48). The RIG-I-like receptors (RLRs) retinoic-acid-inducible gene 1 (RIG-I) and melanoma differentiation-associated gene 5 (MDA5) are expressed in the cytoplasm of all cell types, with the exception of plasmacytoid dendritic cells (pDCs). RIG-I and MDA5 have RNA binding domains and differentially recognize specific characteristics of nonself viral RNAs (17, 22, 36, 37). In addition, RLRs have DExD/H box RNA helicase domains (51) that activate downstream signaling pathways resulting in the activation of IFN regulatory factor 3 (IRF-3) and IRF-7 (53). TLR3 and TLR7 are the sensors for viral double-stranded RNA (dsRNA) and single-stranded RNA, respectively (2, 8, 12). TLR3 is expressed in the endosome of macrophages and conventional dendritic cells (DCs) (28) but not in pDCs. TLR3 is also expressed in a variety of epithelial cells, including airway, uterine, corneal, vaginal, cervical, biliary, and intestinal epithelial cells, which may function as efficient barriers to infection. The TLR3-mediated signaling pathway is transmitted through Toll–interleukin-1 (IL-1) receptor (TIR)-containing adaptor molecule 1, which is also known as TIR domain-containing adaptor inducing IFN-β (TRIF), and finally results in the activation of IRF3 and IRF7 (13, 34, 51). TLR7 is specifically expressed in the endosome of pDCs and contributes to the production of a large amount of IFNs in response to many RNA virus infections (5, 7). TLR7 signaling is mediated by the adaptor molecule myeloid differentiation factor 88 (MyD88). These sensors do not contribute equally

Received 29 May 2011 **Accepted** 20 October 2011
Published ahead of print 9 November 2011
Address correspondence to Satoshi Koike, koike-st@igakuken.or.jp.

doi:10.1128/JVI.05245-11

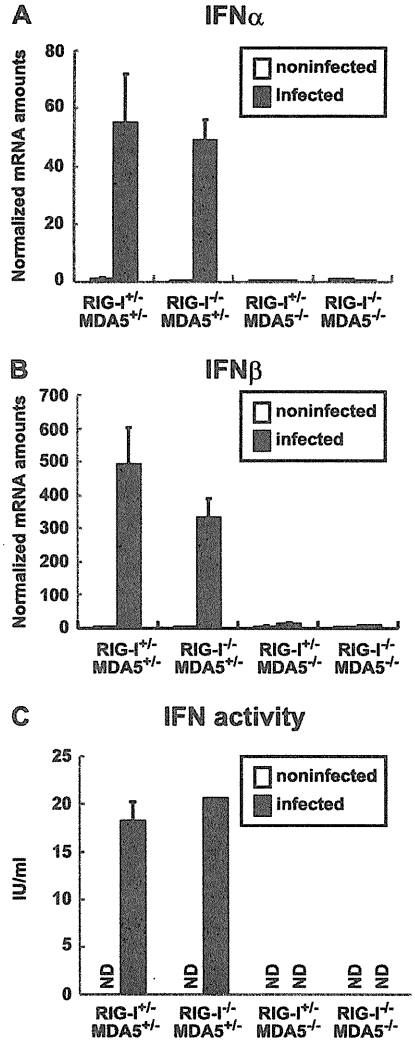

FIG 1 Production of IFNs in primary cultured kidney cells prepared from RIG-I- and MDA5-deficient mice. Kidney cells were pretreated with 100 U of IFN-β for 2 h and infected with PV at an MOI of 10. RNA was prepared from the infected cells at 6 hpi. The amounts of IFN-α mRNA (A) and IFN-β mRNA (B) were determined using quantitative real-time PCR. Cells were prepared in duplicate, and the experiments were repeated three times. Representative data are shown. The amount of IFN activity in the supernatant of infected kidney cells at 8 hpi was determined by the cytopathic effect dye uptake method using L929 cells (C). ND, not detected.

to the antiviral response to each viral infection. The type I IFN production that is induced by these sensors occurs in a virus-specific and cell-specific manner (21, 23). For example, RIG-I plays an important role in the antiviral response to Newcastle disease virus, influenza A virus, Sendai virus, vesicular stomatitis virus, Japanese encephalitis virus, and hepatitis C virus. However, MDA5 is important in the response to infection with picornaviruses, such as encephalomyocarditis virus (EMCV) (10, 23). Although RNA viruses produce dsRNA during the replication step, the protective effect of the TLR3-mediated pathway is not clear (9). In a previous study, TLR3 expression was found to cause severe encephalitis in West Nile virus (WNV) infection (50). How these sensor molecules contribute to the recognition of PV infection is not understood. The aim of the present study was to determine the role of these sensors in the response to PV infection in transgenic mice expressing human PVR. We generated PVR-tg mice deficient in these sensor and adaptor molecules. Our results demonstrate that the MDA5-, TRIF- and MyD88-mediated pathways contribute to the antiviral response against PV infection and that the TLR3-TRIF-mediated pathway plays a pivotal role in this response.

MATERIALS AND METHODS

Cells and viruses. An AGMK cell line, JVK-03 (24), was maintained in Eagle's minimum essential medium containing 5% fetal bovine serum. PV type I Mahoney, a strain derived from the infectious cDNA clone pOM, was used in this study (45). The virus was propagated in JVK-03, and the viral titer was determined using the plaque assay. Primary cultured kidney cells were prepared from transgenic and knockout mice as previously described (54).

Transgenic and knockout mice and infection experiments. All experiments using mice were performed in accordance with the Guidelines for the Care and Use of Laboratory Animals of the Tokyo Metropolitan Institute of Medical Science. ICR-PVRTg21 mice (26) were mated with RIG-I$^{-/-}$ and/or MDA5$^{-/-}$ mice (21) in the ICR background because it is difficult to maintain RIG-I$^{-/-}$ mice in other genetic backgrounds. We mated mice and obtained littermates with the genotypes RIG-I$^{+/-}$ MDA5$^{+/-}$, RIG-I$^{-/-}$ MDA5$^{+/-}$, RIG-I$^{+/-}$ MDA5$^{-/-}$, and RIG-I$^{-/-}$ MDA5$^{-/-}$ to use in experiments. C57BL/6 (B6)-PVRTg21 mice were mated with MDA5$^{-/-}$ mice, TRIF$^{-/-}$ mice, MyD88$^{-/-}$ mice, and TLR3$^{-/-}$ mice (51) in the B6 background (backcrossed 7 to 10 times). IFNAR1$^{-/-}$ PVR-tg mice were previously described (19). Because all of the mice that were used in the present study were in the PVR-tg background, we omitted the notation "PVR-tg" for simplicity in this report. Six- to 7-week-old mice were used for infection experiments. The survival and clinical symptoms of the mice were observed daily for 3 weeks. At the first sign of severe neurological symptoms, the mice were sacrificed as a humane endpoint.

Measurement of IFN levels. IFN-α levels in the sera were determined using an enzyme-linked immunosorbent assay (ELISA). The ELISA kit for IFN-α was purchased from PBL Biochemical Laboratories. Mouse IFN activity in the supernatants of PV-infected kidney cells was measured by the cytopathic effect dye uptake method using L929 cells (54, 55). Recombinant mouse IFN-β (Toray) was used as the standard for unit definition.

Quantitative real-time reverse transcription (RT)-PCR. RNA was isolated from the tissues of infected mice or infected cells using the Isogen RNA extraction kit (Nippon Gene). DNase I treatment and cDNA synthesis were performed as previously described (54). The amounts of the mRNAs for IFN-α, IFN-β, OAS1a, and IRF-7 were determined using real-time RT-PCR with an ABI Prism 7500 (Applied Biosystems) as previously described (54).

RESULTS

IFN production in primary cultured kidney cells is dependent on MDA5. We examined whether, similar to EMCV infection, PV infection is recognized by MDA5 *in vitro*. We mated PVR-tg mice with MDA5-deficient and RIG-I-deficient mice to generate RIG-I$^{+/-}$ MDA5$^{+/-}$, RIG-I$^{-/-}$ MDA5$^{+/-}$, RIG-I$^{+/-}$ MDA5$^{-/-}$, and RIG-I$^{-/-}$ MDA5$^{-/-}$ mice in the ICR background. We prepared primary cultured kidney cells from mice with these genotypes to determine the role of RLRs. After cultivation for approximately 1 week, the cells that became confluent were infected with PV at a multiplicity of infection (MOI) of 10. RNA was recovered from the infected cells at 6 hpi, and the amounts of the mRNAs for IFN-α and IFN-β were determined using real-time RT-PCR. Kid-

ney cells that were not pretreated with IFN-β before PV infection showed rapid cytopathic effect progression and did not produce IFN mRNA (data not shown). This result is consistent with our previous observations (54). We therefore pretreated cells with 100 U of IFN-β for 2 h and infected them with PV. As we reported previously, the IFN-treated kidney cells became resistant to PV infection, PV replication was severely inhibited, and IFN production was observed (54). Under this condition, we determined the sensor responsible for IFN production. We observed the induction of both IFN-α (Fig. 1A) and IFN-β mRNAs (Fig. 1B) in cells that were isolated from RIGI-I$^{+/-}$ MDA5$^{+/-}$ mice and RIGI-I$^{-/-}$ MDA5$^{+/-}$ mice but not from RIGI-I$^{+/-}$ MDA5$^{-/-}$ mice or RIGI-I$^{-/-}$ MDA5$^{-/-}$ mice. The induced IFN proteins were not detected by ELISA due to a very small amount of IFNs produced in the supernatants. However, IFN activity was detected in the supernatants of PV-infected kidney cells prepared from RIGI-I$^{+/-}$ MDA5$^{+/-}$ mice and RIGI-I$^{-/-}$ MDA5$^{+/-}$ mice but not from RIGI-I$^{+/-}$ MDA5$^{-/-}$ mice or RIGI-I$^{-/-}$ MDA5$^{-/-}$ mice using the cytopathic effect dye uptake method (Fig. 1C). These results suggest that PV infection is recognized by MDA5 but not RIG-I in primary murine kidney cells, which is consistent with previous reports demonstrating that MDA5 is essential for the detection of picornaviruses (10, 23). However, MDA5-mediated IFN production was observed only when cells had been primed with a low dose of IFNs.

IFN responses of MDA5-deficient mice are not significantly different from those of wild-type mice. We hypothesized that MDA5 plays an important role in the type I IFN response upon PV infection *in vivo*. We examined the serum IFN-α levels in PVR-tg mice intravenously infected with 2×10^7 PFU of PV using ELISA. Their serum IFN-α level was initially observed at 9 hpi, peaked at 12 hpi, and began to decline at 24 hpi (Fig. 2A). We then determined the serum IFN-α levels of the knockout mice at 12 hpi. Unexpectedly, similar serum IFN-α levels were detected in RIG-I$^{+/-}$ MDA5$^{+/-}$, RIG-I$^{+/-}$ MDA5$^{-/-}$, RIG-I$^{-/-}$ MDA5$^{+/-}$, and RIG$^{-/-}$ MDA5$^{-/-}$ mice infected with PV (Fig. 2B).

We monitored the induction of mRNAs for the IFN-stimulated genes (ISGs), OAS1a (Fig. 3A) and IRF-7 (Fig. 3B), in the brain, spinal cord, liver, spleen, and kidney using real-time RT-PCR. Among the organs tested, the expression levels of these ISGs were the highest in the spleen. However, the expression profiles of these genes were essentially the same in all organs. In accordance with the elevated serum IFN levels, the induction of ISGs in various organs was observed in all mice (Fig. 3A and B). The results suggest that MDA5 does not play a critical role in IFN production and subsequent ISG induction in response to PV infection *in vivo*.

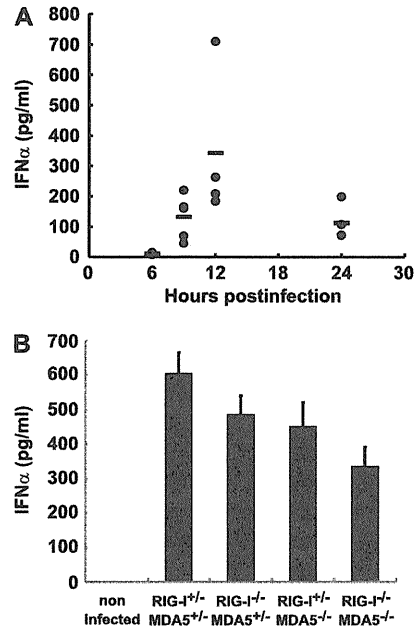

FIG 2 Production of serum IFN-α in RIG-I- and MDA5-deficient mice. (A) Time course of IFN-α levels in serum. PVR-tg mice in the B6 background (n = 4 or n = 5) were intravenously infected with 2×10^7 PFU of PV. Serum samples were collected at the indicated time points, and the concentration of IFN-α was determined using ELISA. (B) IFN-α levels of RIG-I- and MDA5-deficient mice in the ICR background (n = 8) at 12 hpi were compared. The experiments were repeated twice, and representative data are shown.

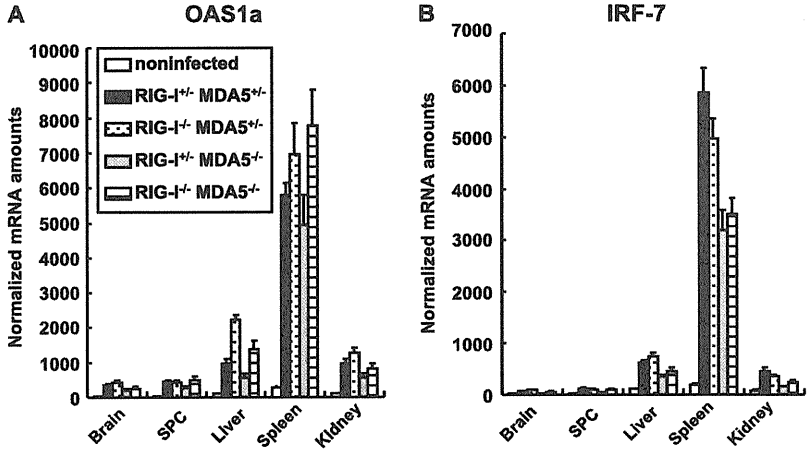

FIG 3 ISG induction in RIG-I- and MDA5-deficient mice. Mice (n = 4) were intravenously infected with 2×10^7 PFU of PV. At 12 hpi, RNA was isolated from the indicated tissues of the infected mice and OAS1a (A) and IRF-7 (B) mRNA levels were determined using quantitative real-time PCR. The experiments were repeated twice, and representative data are shown. SPC, spinal cord.

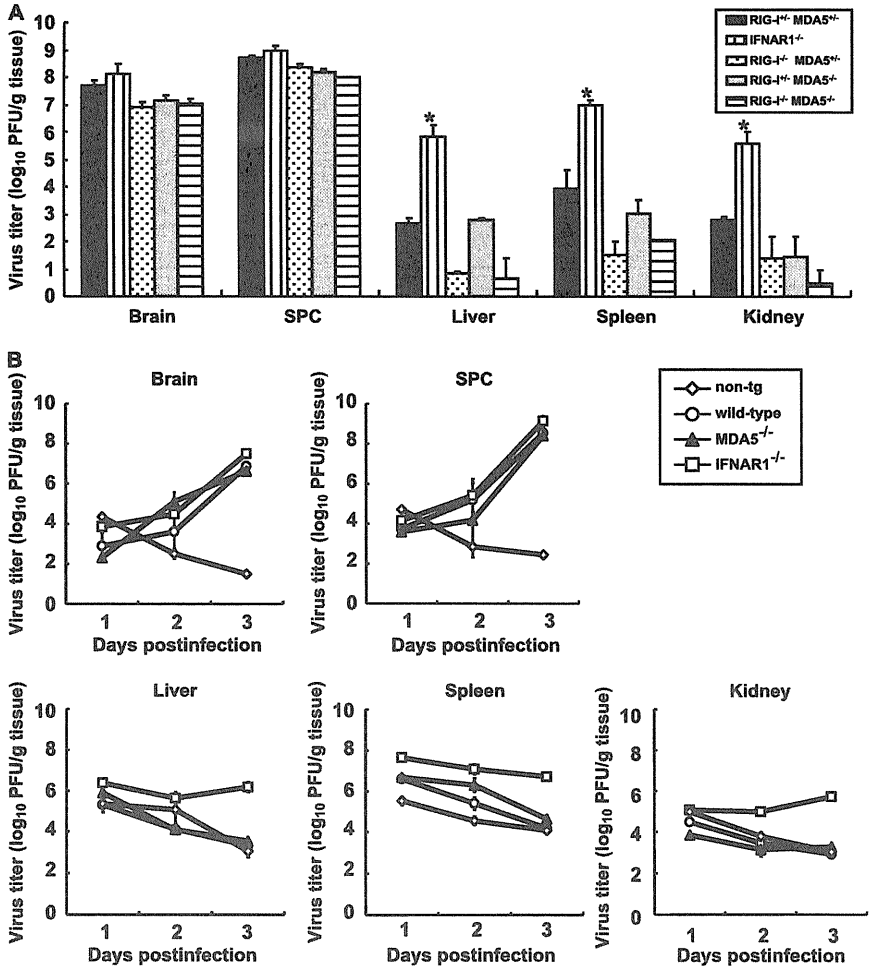

FIG 4 (A) PV replication in RIG-I- and MDA5-deficient mice. RIGI-$I^{+/-}$ $MDA5^{+/-}$, RIGI-$I^{-/-}$ $MDA5^{+/-}$, RIGI-$I^{-/-}$ $MDA5^{+/-}$, and RIGI-$I^{-/-}$ $MDA5^{-/-}$ mice in the ICR background and $IFNAR1^{-/-}$ mice in the B6 background ($n = 3$) were intravenously infected with 2×10^7 PFU of PV. Infected mice were paralyzed or dead at 3 to 5 days postinfection. The tissues of the paralyzed mice were collected, and the viral titers were determined using a plaque assay (*, $P < 0.01$ by t test compared to RIGI-$I^{+/-}$ $MDA5^{+/-}$ mice). (B) PV replication kinetics in MDA5-deficient mice. Nontransgenic (non-tg) mice, wild-type mice, $MDA5^{-/-}$ mice, and $IFNAR1^{-/-}$ mice in the B6 background ($n = 3$) were infected as described above. Tissues were collected daily, and viral titers were determined. SPC, spinal cord.

PV replication in nonneural tissues and mortality rates of mice deficient in RIG-I-like receptors. We have previously shown that the IFN-α/β response forms an innate immune barrier to prevent PV replication in nonneural tissues and PV invasion of the CNS (19, 25). Therefore, we evaluated PV replication in neural and nonneural tissues in RLR-deficient mice. The mice were infected with 2×10^7 PFU of PV, which is approximately 100 times higher than the 50% lethal doses for all mouse strains. The infected mice showed paralysis by 3 to 5 days postinfection. The brain, spinal cord, liver, spleen, and kidney of the paralyzed mice were recovered, and their viral titers were determined (Fig. 4A). PV was recovered from the CNS of the paralyzed mice almost equally among the genotypes. The viral titers recovered from the liver, spleen, and kidney of $IFNAR1^{-/-}$ mice were significantly higher than those of wild-type mice, as previously described (19). However, PV titers that were recovered from these organs of RIG-$I^{-/-}$ $MDA5^{+/-}$, RIG-$I^{+/-}$ $MDA5^{-/-}$, and RIG-$I^{-/-}$ $MDA5^{-/-}$ mice were as low as or lower than those in the organs of RIG-$I^{+/-}$ $MDA5^{+/-}$ mice. We then examined virus replication kinetics using nontransgenic mice, wild-type mice, $IFNAR^{-/-}$ mice, and $MDA5^{-/-}$ mice in the B6 background (Fig. 4B). The viral load in the CNS increased in a similar fashion among the transgenic mouse strains. However, the viral load kinetics in the liver, spleen, and kidney of wild-type and $MDA5^{-/-}$ mice were similar to those of nontransgenic mice. The values for nontransgenic mice indicate the kinetics of clearance of inoculated virus. The results indicated that PV replication was severely inhibited in the liver, spleen, and kidney of wild-type and $MDA5^{-/-}$ mice. This inhibition correlated well with the induction of serum IFNs in $MDA5^{-/-}$ mice (Fig. 2). The PV antigen was detected in neurons in the CNS but not in other tissues in all knockout mice (Table 1). This result indicates that the lack of RLRs did not alter the tissue tropism of PV. These data suggest that inhibition of PV replication in nonneural tissues is not dependent on RLRs and that MDA5-independent mechanisms are the major contributors in controlling PV replication.

We examined the mortality rates of RIG-$I^{+/-}$ $MDA5^{+/-}$, RIG-$I^{-/-}$ $MDA5^{+/-}$, RIG-$I^{+/-}$ $MDA5^{-/-}$, and RIG-$I^{-/-}$ $MDA5^{-/-}$